Enhanced oxidation of arsenite to arsenate using tunable K^+ concentration in the OMS-2 tunnel

by Hou, J., Sha, Z., Hartley, W., Tan, W., Wang, M., Xiong, J., Li, Y., Ke, Y. Long, Y. and Xue, S.

DOI: https://doi.org/10.1016/j.envpol.2018.03.047

Hou, J., Sha, Z., Hartley, W., Tan, W., Wang, M., Xiong, J., Li, Y., Ke, Y. Long, Y. and Xue, S. 2018. Enhanced oxidation of arsenite to arsenate using tunable K^+ concentration in the OMS-2 tunnel. *Environmental Pollution,* 238, pp.524-531.

Enhanced oxidation of arsenite to arsenate in K^+ doped manganese oxide OMS-2 tunnel structures

Jingtao Hou [a, b *], Zhenjie Sha [a], William Hartley [c], Wenfeng Tan [a], Mingxia Wang [a], Juan Xiong [a], Yuanzhi Li [b], Yujie Ke [d], Yi Long [d], Shengguo Xue [e, f]

[a] Key Laboratory of Arable Land Conservation (Middle and Lower Reaches of Yangtse River), Ministry of Agriculture, College of Resources and Environment, Huazhong Agricultural University, Wuhan, 430070, China.

[b] State Key Laboratory of Silicate Materials for Architectures Wuhan University of Technology, Wuhan, 430070, China.

[c] Crop and Environment Sciences Department, Harper Adams University, Newport, Shropshire, TF10 8NB, United Kingdom

[d] School of Materials Science and Engineering, Nanyang Technological University, 50 Nanyang Avenue, Singapore 639798, Singapore

[e] Department of Environmental Engineering, School of Metallurgy and Environment, Central South University, Changsha, 410083, China.

[f] Chinese National Engineering Research Centre for Control and Treatment of Heavy Metal Pollution, Changsha 410083, China

Corresponding author:

* Email: jthou@mail.hzau.edu.cn (J. T. H.), Telephone: +86-27-8728 7508.

ABSTRACT

Manganese oxide cryptomelane-type octahedral molecular sieves (OMS-2) possess a high redox potential and the ability to oxidize arsenite (As(III)) to arsenate (As(V)) in order to reduce its toxicity and removal. However, coexisting ions such as phosphate are ubiquitous and readily bond to manganese oxide surfaces, consequently passivating surface active sites and reducing As(III) oxidation. In this study, we present a novel strategy to significantly promote As(III) oxidation activity by OMS-2 by tuning the K^+ concentration. Batch experimental results reveal that increasing the K^+ concentration not only considerably improved As(III) oxidation kinetics from 0.027 to 0.102 min^{-1}, but also reduced the adverse effect of competitive ions on As(III) oxidation. Arsenite oxidation was investigated through As(V) and phosphate adsorption kinetics, detection of Mn^{2+} release in solution, surface charge characteristics, and density functional theory (DFT) calculations. Experimental results and theoretical calculations confirm that by increasing K^+ concentrations in the OMS-2 tunnel structure, not only does it improve arsenic adsorption on K^+ doped OMS-2, but also accelerates two electron transfers from As(III) to each bonded Mn atom on OMS-2 surfaces, and as a result, considerably improves As(III) oxidation rate, which is responsible for counteracting adsorption by coexisting ions.

Keywords: OMS-2; K^+ doping; Arsenite oxidation; Arsenate; Competitive adsorption

Main findings of the work

We present a novel strategy to promote As(III) oxidation kinetic rate and counteract the adverse effects of coexisting ions on As(III) oxidation by tuning K^+ content in the OMS-2 tunnel structure.

1 Introduction

Arsenic (As) has received much attention due to its toxicity and carcinogenicity, even at concentrations of up to 10 μg L^{-1}. In As-contaminated groundwater, As is mainly present in its inorganic state, with arsenate [As(V)] and arsenite [As(III)] being the two predominant species. It has been reported that the emission of waste As species in many industrial processes such as metallurgic industries, mainly exists as As(III) species, which is very stable in aqueous environments under slightly reducing conditions (Gutiérrez-Ruíz et al., 2005). Since As(III) has greater toxicity, but weaker adsorption characteristics compared to As(V) (Ventura-Lima et al., 2011), oxidation of As(III) to As(V) is a desirable process, in order to reduce As toxicity and promote total As removal. However, oxygen-driven oxidation of As(III) is reportedly very slow in groundwater, having reaction kinetic half-times in the range of several months to a year (Gorny et al., 2015). Therefore, additional oxidants are still required for the efficient oxidation of As(III) prior to treatment by coprecipitation and adsorption (Mondal et al., 2013).

Manganese oxides are ubiquitous in terrestrial environments and possess high redox potentials (Fischel et al., 2015; Villalobos et al., 2014), being highly efficient oxidants of As(III), potentially promoting total As removal (Chakravarty et al., 2002; Chen et al., 2018; Deschamps et al., 2005; Maliyekkal et al., 2009; Neumann et al., 2013; Zhang et al., 2013, 2007). For example, Zhang et al (2013) observed that synthetic Fe-Mn binary oxides had a high removal capacity for As(III), which was attributed to the oxidation ability of manganese oxides for As(III), but also As(V) adsorption by iron oxides (Zhang et al., 2014, 2007). Deschamps et al (2005) evaluated both As(III) and As(V) removal from groundwater using a natural Fe and Mn enriched ore (denoted as cFeMn) through batch and column experiments (Deschamps et al., 2005). They revealed that cFeMn (45% Fe_2O_3 and 35% MnO_2) demonstrated efficient removal of 100 μg L^{-1} As(III) to the drinking water standard when total throughput was lower than 7400 BV (Bed Volume). Although both synthetic Fe-Mn binary oxides and Fe and Mn enriched samples present highly efficient removal of As(III), their As(III) oxidation kinetic rates are very slow, i. e., As(III) can be completely oxidized to As(V) only after 8 h (Zhang et al., 2007) and 50 h (Deschamps et al., 2005), respectively. It is well known that widespread coexisting ions, such as phosphate, readily bind to manganese oxide surface active sites, and these may hinder As(III) adsorption and subsequently impede their oxidation (Hou et al., 2017, 2016; Lafferty et al., 2010). Therefore, it is of scientific and technological importance to

seek a novel approach to improving As(III) oxidation rate on manganese oxides by reducing the adverse effects of coexisting ions. It is commonly accepted that As(III) species adsorb onto manganese oxides forming a bidentate complex, subsequently two electrons transfer from As(III) to Mn(IV), and this results in the production of As(V) and Mn^{2+} ions (Moore et al., 1990; Nesbitt et al., 1998). Arsenic adsorption and As(III) electron transfer rate must be explored further in order to improve As(III) oxidation rate and accelerate electron transfer from As(III) to Mn.

Cryptomelane-type manganese oxide (OMS-2) possesses a 2 × 2 tunnel structure formed by edge- and corner-shared MnO_6 octahedra, and has attracted interest due to its ability to oxidize As(III) (Hou et al., 2016; Li et al., 2010; Wang et al., 2012). Since K^+ ions are similar to the dimensions of 2 × 2 tunnel structures, they have been used as an ideal template for synthetizing manganese oxide with 2 × 2 tunnel structures in the laboratory (Liu et al., 2003). Generally, naturally occurring OMS-2 essentially exist as K^+ ions in tunnel structures having variable contents. Thus, the varying K^+ concentrations in OMS-2 tunnels inadvertently change their chemical and physical properties, such as magnetic properties and catalytic performance for pollutant purification, which has been observed in previous reports (Hou et al., 2013; Luo et al., 2010). Nevertheless, insufficient work has been reported on K^+ concentration effects, on As(III) oxidation using OMS-2 in terrestrial environments. The mechanism for K^+ ion As(III) oxidation on OMS-2 still remains unanswered. To summarize, understanding the relationship between OMS-2 structure with variable K^+ contents and As(III) oxidation activity, will provide important insights into the transport and fate of toxic As(III) in natural environments.

Consequently, K^+ doped OMS-2 tunnel structures were used to oxidize As(III) to As(V) in this study. For the first time, we observed a significant effect on As(III) oxidation using variable K^+ concentrations with OMS-2. Increasing K^+ concentration in tunnel structures promoted As(III) oxidation whilst reducing the adverse effect of coexisting ions such as As(V) and phosphate. We also revealed the origin of the effect of K^+ concentration in the tunnel of OMS-2 on As(III) oxidation by combining both experimental and theoretical evidence.

2. Experimental section

2.1. Sample preparation

K^+ doped OMS-2 samples were synthesized using a superficial hydrothermal redox reaction with $MnSO_4$, $(NH_4)_2S_2O_8$, and $(NH_4)_2SO_4$ by adding variable KNO_3 concentrations at 120 °C for 24 h. The methodology is described in previous work (Hou et al., 2013). Potassium nitrate (KNO_3) (0, 0.4044, 1.6176 g respectively) were added to the reaction solutions which corresponded to $KNO_3/MnSO_4$ molar ratios of 0, 0.5, and 2, respectively. The samples were subsequently symbolized as K-OMS-2-A, K-OMS-2-B and K-OMS-2-C, respectively.

2.2. Batch experimental procedures

Batch experiments for As(III) oxidation using K^+ doped OMS-2 samples were performed using a water-bathing rotary oscillator at 160 rpm, at 25 °C. Arsenite was prepared from a $NaAsO_2$ stock solution to give a 100 μM working solution. Detailed experimental procedures are described in previous work (Hou et al., 2016). The coexisting ions of As(V), phosphate, and Mn^{2+} that affect As(III) oxidation were evaluated by adding 100 μM of $Na_2HAsO_4{\cdot}7H_2O$, NaH_2PO_4, and $Mn(NO_3)_2$ into 100 μM As(III) solution, respectively. pH effect was investigated using buffer solutions at pH 4.7, 6.0 and 9.16, respectively. An acetate acid/sodium acetate buffer system was used to adjust pH to 4.7 and 6.0. A sodium carbonate/sodium bicarbonate buffer system was used to control pH at 9.16. Detailed procedures of the buffer systems are described in previous work (Hou et al., 2016).

2.3. Analysis methods

The concentrations of total As and As(V) in solution were detected using colorimetric spectrophotometry. Arsenite concentration in solution was determined by subtracting As(V) from the total As concentration. Detailed procedures are described in previous work (Hou et al., 2016). When phosphate was present in solution, the concentrations of As(III) and total As species were obtained by hydride generation (LH-2A) atomic absorption spectrophotometry (AAS-6880); detailed procedures are described in previous work (Hou et al., 2016). Dissolved Mn^{2+} concentrations were determined by AAS (6880). Potassium was determined by inductively coupled plasma optical emission spectroscopy (ICP-OES, PerkinElmer Optima 4300DV). Redox potential (Eh) was measured using a CHI660B electrochemical workstation at 25 °C. Platinum and reference electrodes (saturated calomel electrode) were selected as combination electrodes. Eh values

were adjusted by a standard hydrogen electrode (SHE) to obtain true Eh values.

2.4. Isoelectric point test

The isoelectric point (IEP) of K^+ doped OMS-2 samples were determined on a zeta potential analyzer (Zetasizer Nano, ZEN3600, Malvern Instruments Ltd., U.K) (Wan et al., 2016; Yan et al., 2014). Typically, each sample (2.5 mg) was added to distilled water (500 mL) and sufficiently dispersed through ultrasonication for 0.5 h. A series of 20 ml suspensions (5.0 mg L^{-1}) were then transferred to centrifuge tubes (50 mL) and 0.1 mol L^{-1} HCl or 2.5 mol L^{-1} NaOH was used to adjust suspension pH to the target values between 2.0 to 7.0. Each suspension was kept for 1 day at 25 ºC to ensure pH remained stable. Zeta potential was tested three times. IEP's were determined from zeta potential plots against pH, where zeta potential was zero. pH values of the suspensions were tested on a Mettler Toledo pH meter (FiveEasy Plus FE20) with a measurement accuracy of 0.01.

2.5 DFT calculation

A Density functional theory (DFT) calculation was employed to investigate adsorption energy of As species on K-OMS-2 surfaces ($K_xMn_8O_{16}$). The Vienna Ab-initio Simulation Package (VASP) was used to perform DFT calculations. A bidentate-binuclear adsorption model of arsenic species on OMS-2 supercells (~ 100 atoms) was constructed according to Manning et al., (2002) and Zhu et al., (2009). To reveal any K^+ concentration effect on As species, $K_2Mn_{32}O_{64}$ and $K_4Mn_{32}O_{64}$ were incorporated into the tunnel of the OMS-2 supercell. The method of DFT calculations is described in previous work (Hou et al., 2013). A 2 × 2 × 2 Monkhorst-Pack k-point mesh was used to optimize the OMS-2 supercell structure. Kinetic cutoff energy was set to 400 eV. The convergence criteria of the electronic and ionic relaxations were set to 10^{-4} eV and 0.02 eV $Å^{-1}$, respectively.

3. Results and discussion

3.1. Sample Characterization

K^+ doped OMS-2 samples in the tunnel were synthesized using a superficial hydrothermal redox reaction between $MnSO_4$, $(NH_4)_2S_2O_8$, $(NH_4)_2SO_4$, and KNO_3 at 120 ºC for 24 h, in which $KNO_3/MnSO_4$ reactant molar ratios ranged from 0 to 0.5 and 2, respectively (Hou et al., 2013). The samples were labeled as K-OMS-2-A, K-OMS-2-B, and K-OMS-2-C. XRD patterns revealed that the prepared samples had the same cryptomelane structure (OMS-2, $K_xMn_8O_{16}$)

(JCPDS-29-1020) (Fig. S1, Supporting information). ICP-OES analysis revealed that K^+ concentrations in the OMS-2 tunnel increased with an increase in the initial $KNO_3/MnSO_4$ reactant molar ratio (Table 1). The K/Mn molar ratios of K-OMS-2-A, K-OMS-2-B, and K-OMS-2-C, were 0, 0.03, and 0.07, respectively (Table 1). The K/Mn molar ratios of K-OMS-2-A, K-OMS-2-B, and K-OMS-2-C obtained by XPS analysis were very close to those determined by ICP-OES, i. e., 0, 0.04, and 0.08, respectively (Table 1). TEM and HRTEM mappings revealed that all K^+ doped OMS-2 samples had nanorod-like morphologies with uniformly exposed {200} facets (Hou et al., 2013). The BET specific surface area of K-OMS-2-A, K-OMS-2-B, and K-OMS-2-C, as calculated from N_2 adsorption or desorption curves, were 65.1, 89.2, and 109.7 $m^2 g^{-1}$, respectively (Table 1).

3.2. As(III) oxidation performance

Results of As(III) oxidation by K^+ doped OMS-2 are presented in Fig. 1A. Without doping, K-OMS-2-A revealed the lowest As(III) oxidation activity, with 64.5% arsenite oxidation after 30 min. Increasing the tunnel K^+ concentration lead to a considerable increase in As(III) oxidation. Arsenite oxidation by K-OMS-2-B (high K^+ concentration) increased from 64.5% to 83.0% after 30 min. K-OMS-2-C (greatest K^+ concentration) revealed the highest As(III) oxidation activity, with 95.5% arsenite being oxidized to As(V) after 30 min (Fig. 1A). To determine whether dissolved oxygen affected As(III) oxidation, a control study using As(III) in the absence of OMS-2 was carried out at pH 6.0. After 30 minutes there was no change in oxidation state (Fig. 1A) indicating that dissolved oxygen was not involved in this process, which is in agreement with previous work (Lan et al., 2018). The K^+ release in K-OMS-2-C during As(III) oxidation was also examined by ICP-OES analysis. As shown in Fig S2, K^+ concentration was not detected at the initial stage (10 min), but after 30 min, there was a small release of 3.1 wt% (corresponding to the fraction of total K^+ content in K-OMS-2-C), which may be due to the reductive dissolution of manganese oxide during As(III) oxidation (Manning et al., 2002; Nesbitt et al., 1998). This result indicates that K^+ located in the OMS-2 tunnel is stable in our case. Arsenite oxidation by manganese oxide reportedly follows first-order kinetics at the initial reaction stage (e. g., 30 min) (Manning et al., 2002). Thus, As(III) oxidation kinetics rate constants (k_{oc}) for different samples were obtained by fitting a first-order kinetics equation. As shown in Fig. 1B, K-OMS-2-A presents the lowest k_{oc}, i. e., 0.027 min^{-1}. For K-OMS-2-B, its k_{oc} increases to 0.059 min^{-1}. K-OMS-2-C possesses the highest k_{oc} (0.102 min^{-1}), which is 1.73 and 3.7

180 times greater than those of K-OMS-2-A and K-OMS-2-B, respectively. This result demonstrates that K^+ concentration in
181 the OMS-2 tunnel has a significant effect on As(III) oxidation.

182 It is well known that As(III) species do not exist alone, but coexist with As(V) species due to varying redox conditions
183 in aqueous and soil environments (Gorny et al., 2015; Smedley and Kinniburgh, 2002). Therefore, the effect of
184 competitive adsorption must be considered, once K-OMS-2 is used as an oxidant for treating toxic As(III) in real arsenic
185 polluted groundwater. Although previous literature has reported that coexisting As(V) has adverse effects on As(III)
186 oxidation, to date, a limited number of studies have focused on how to reduce the adverse effect of coexisting As(V) on
187 As(III) oxidation by manganese oxide (Hou et al., 2017b, 2016). To evaluate whether As(V) affects As(III) oxidation on
188 K-OMS-2, we added 100 μM As(V) into 100 μM As(III) solution. Fig. 2A reveals that As(III) removal by K-OMS-2-A
189 decreased from 64.5% to 43.2% after addition of 100 μM As(V), which was reduced by 20.2%. Increasing K^+
190 concentration in the OMS-2 tunnel lead to a decrease in the adverse effect of As(V) on As(III) oxidation. For
191 K-OMS-2-B (high K^+ concentration), As(III) removal was reduced from 14.3% to 68.4% after the addition of 100 μM
192 As(V). Whereas for K-OMS-2-C (greatest K^+ concentration), As(III) removal was 94.9% after the addition of 100 μM
193 As(V), which was only reduced by 0.6%, suggesting As(V) had no obvious effect on As(III) removal by K-OMS-2-C.
194 This result suggests that the strategy of doping K^+ in the OMS-2 tunnel is a practicable approach to significantly
195 reducing the adverse effect of coexisting As (V) on As(III) oxidation.

196 The question in our case, is why coexisting As(V) had no clear effect on As(III) oxidation by K-OMS-2-C? Two
197 considerations which may affect As(III) oxidation by K-OMS-2 include, (a) As(III) oxidation rate kinetics (Hou et al.,
198 2017b, 2016) and (b) favorable adsorption of competitive coexisting ions, which obstruct the contact between As(III) and
199 K-OMS-2 surfaces, and thereby reduce As(III) oxidation rate (Lafferty et al., 2010). In order to determine whether the
200 effect of As(V) on As(III) oxidation arises because As(V) adsorption is preferential, we evaluated As(V) adsorption
201 capacity on three samples. Arsenate adsorption efficiency for K-OMS-2-A, K-OMS-2-B, and K-OMS-2-C was 52.5%,
202 71.4%, and 79.3%, respectively (Fig. 2B), suggesting that As(V) species can adsorb onto all the OMS-2 samples.
203 Therefore, a reduction in As(III) oxidation on K-OMS-2-A and K-OMS-2-B following the addition of As(V), may arise
204 from occupation and passivation of OMS-2 surface active sites by As(V). In principle, the greater the As(V) adsorbtion

onto K-OMS-2, the lower the As(III) removal rate is. Unusually, although K-OMS-2-C demonstrated greater As(V) adsorption capacity (68.7 μmol g^{-1}) than K-OMS-2-B (61.9 μmol g^{-1}) and K-OMS-2-A (45.5 μmol g^{-1}) (Fig. 2B), competitive adsorption of coexisting As(V) had a limited effect on As(III) oxidation (Fig. 2A). The main reason for this may be attributed to the greater As(III) oxidation kinetic rate of K-OMS-2-C in comparison to K-OMS-2-A and K-OMS-2-B (Fig. 3). Consequently, rapid As(III) oxidation kinetic rates play a vital role in counteracting the adverse effects of coexisting As(V) adsorption, thus considerably enhancing As (III) oxidation on K-OMS-2-C.

Phosphate has a structure similar to arsenate and was selected as a competitive ion to further understand the effect of competitive adsorption of As(III) oxidation on K-OMS-2 samples. For K-OMS-2-B and K-OMS-2-A samples, following addition of 100 μM phosphate, As(III) removal decreased to 65.0% and 45.1%, respectively, being reduced by 17.7% and 20.8% as compared to that of no addition (Fig. 3A). This was also observed in previous works, and has been attributed to favorable adsorption of phosphate species onto active sites (Chiu and Hering, 2000; Lafferty et al., 2010). For K-OMS-2-C, As(III) removal was 93.1% after addition of 100 μM phosphate, which was close to that of no phosphate (95.5%), indicating that the presence of phosphate species had no obvious effect on As(III) oxidation by K-OMS-C in this case. Phosphate adsorption kinetic rate constants (k_{ac}) of K-OMS-2 samples were obtained by fitting both pseudo-first-order and pseudo-second-order models at a phosphate concentration of 100 μM (Fig. 3B). The fitting formulae for the two models are described in a previous report (Hou et al., 2017a). It can be seen that phosphate rapidly adsorbed onto OMS-2 surfaces at the initial stage and subsequently reached adsorption equilibrium after 200 min (Fig. 3B). Phosphates adsorption kinetic rate on K-OMS-2-A, K-OMS-2-B and K-OMS-2-C, obtained by fitting a fist-order model, were 0.075, 0.079, and 0.088 min^{-1}, respectively (Table S1). For K-OMS-2-A and K-OMS-2-B, phosphate adsorption kinetic rates are larger than their corresponding As(III) oxidation kinetic rates (0.027 and 0.059 min^{-1}, respectively). This has revealed that phosphate adsorption on K-OMS-2-A and K-OMS-2-B surfaces is faster than As(III) oxidation, leading to fast occupation of OMS-2 surfaces and reducing As(III) oxidation. The phosphate adsorption kinetic rate of K-OMS-2-C was lower than As(III), revealing that As(III) oxidation was faster, and thereby counteracting the adverse effects of phosphate adsorption. This demonstrates that the highly efficient As(III) oxidation on K-OMS-2-C in the presence of coexisting ions is attributed to its rapid As(III) oxidation kinetic rate.

As a result of re-adsorption of dissolved Mn^{2+} onto manganese oxide surfaces (Lafferty et al., 2011), a decrease in As(III) removal by OMS-2 may occur. Therefore, 100 μM Mn^{2+} was added to the As(III) solution, and K-OMS-2-B and K-OMS-2-A reduced it to 70.9% and 49.5%, respectively, whereas K-OMS-2-C removed 93.5%, having no obvious change compared to no Mn^{2+} addition (Fig. 3A). This result reveals that doping K^+ in the OMS-2 tunnel is an approach to fast oxidation of As(III) to As(V) and for opposing the adverse adsorption effect of coexisting ions such as Mn^{2+}.

The effect of phosphate and Mn^{2+} was also evaluated at different concentrations (0.1, 1.0, and 4.0 mM) on As(III) oxidation by K-OMS-2-C at pH 6.0 (Fig. S3). Following phosphate addition at 1.0 mM, As(III) removal by K-OMS-2-C (87.1%) was lower than that at 0.1 mM (93.1%). A further increase in phosphate, from 1.0 to 4.0 mM, resulted in As(III) removal being reduced from 87.1% to 75.0% (Fig. S3). There are two possible reasons that may be responsible for interpreting why higher phosphate concentration blocks As(III) oxidation on K-OMS-2-C, even if it has a high As(III) oxidation kinetic rate. Firstly, the phosphate adsorption kinetic rate increased with increasing phosphate concentration in solution (Hou et al., 2017b), and once phosphate adsorption was close to that of the As(III) oxidation kinetic rate, phosphate adsorption by K-OMS-2-C is observed (Hou et al., 2017b). Secondly, a change in redox potential (Eh) following phosphate addition may affect adsorption rate on K-OMS-2-C. Nevertheless, in the presence of low or high phosphate concentration, Eh does not significantly change, and the increase in phosphate adsorption kinetic rate at high phosphate concentration (e. g., 1.0 and 4.0 mM) plays the major role in reducing As(III) oxidation rate (Fig S4). For Mn^{2+} ions, it was revealed that a similar range in phosphate affects As(III) oxidation by K-OMS-2-C. After adding Mn^{2+} from 0.1 mM to 1.0 and 4.0 mM, As(III) removal by K-OMS-2-C decreased from 93.5% to 53.0% and 45.9%, respectively (Fig. 4), indicating that the Mn^{2+} effect on As(III) oxidation was greater than that of phosphate at high concentration.

The effect of dosage and initial As(III) concentration on K-OMS-2-C As(III) oxidation was investigated at pH 6.0 (Fig. S5). Arsenite removal increased with increasing K-OMS-2-C dosage and decreased the initial As(III) concentration (Fig. S5). The pH effect on As(III) removal by K-OMS-2-C was also examined by controlling solution pH to 4.7, 6.0, and 9.16, respectively (Fig. S6). Arsenite removal at 4.7, 6.0, and 9.16 was 93.7, 95.5, and 97.4%, respectively (Fig. S6). Although As(III) removal at pH 9.16 was greater than at pH 6.0 and 4.7, K-OMS-2-C still showed greater As(III)

oxidation activity at pH 6.0 and 4.7 (93.0%), indicating that K-OMS-2-C possesses wide pH adaptability in acid, neutral, and alkaline conditions, and is very important for its application in As(III) oxidation.

3.3. Origin of K^+ concentration effect on As(III) oxidation by OMS-2

3.3.1 Specific surface area

The calculated As(III) oxidation rates of K^+ doped OMS-2 samples are presented in Table 1. Arsenite oxidation rates of K-OMS-2-A, K-OMS-2-B, and K-OMS-2-C were 2.96, 4.29, and 7.78 μmol g^{-1} min^{-1}, respectively. As they have different specific surface areas, specific As(III) oxidation rates, defined as the content of reacted As(III) per unit surface area per unit time, were compared (Table 1). For K-OMS-2-C, the greatest specific As(III) oxidation rate (0.071 μmol m^{-2} min^{-1}), was 1.4 and 1.6 times higher than K-OMS-2-B and K-OMS-2-A.

3.3.2 Surface charge characteristics

To investigate the effect of K^+ concentration on surface charge characteristics, zeta potentials were tested. As shown in Fig. 4, zeta potentials decreased with increasing pH in suspensions. Zeta potentials of all suspensions at pH 6.0 (i. e., batch experimental conditions of As(III) oxidation in this work) were negative values, indicating As species (e. g., AsO_3^{3-} and AsO_4^{3-}) are unfavorable to adsorption on OMS-2 surfaces due to electrostatic repulsion. For K-OMS-2-A, its isoelectric point (IEP) was 4.22 (Fig. 4). Remarkably, increasing K^+ concentration in the OMS-2 tunnel led to a considerable increase in IEP values. For K-OMS-2-B, its IEP value increased to 4.95 whereas K-OMS-2-C possessed the largest IEP value, 5.37. This indicated that increasing K^+ concentration causes IEP values to shift in high pH, thereby reducing the electrostatic repulsion and facilitating As adsorption at neutral pH range (e. g., pH at 6.0).

3.3.3 Detection of dissolved Mn^{2+} in solution

According to the mechanism of As(III) oxidation on manganese oxide as described in the introduction, the faster the electron transfer rate from arenite to Mn atoms in K^+ doped OMS-2, the faster is the As(III) oxidation rate and the larger is the dissolved Mn^{2+} ion concentration in solution. Therefore, the change in dissolved Mn^{2+} concentration, as a function of reaction time, was recorded to evaluate As(III) electron transfer rate of different K^+ doped OMS-2 samples. As shown in Fig. 5, for K-OMS-2-A, the dissolved Mn^{2+} concentration in solution was 0.020 mmol L^{-1}. Increasing K^+ concentration led to an increase in dissolved Mn^{2+} concentration in solution. For K-OMS-2-B with high K^+ concentration,

the dissolved Mn^{2+} concentration increased to 0.037 mmol L^{-1} after 30 min. For K-OMS-2-C with the highest K^+ concentration, the dissolved Mn^{2+} concentration increased further to 0.049 mmol L^{-1} after 30 min. The non-stoichiometric Mn^{2+} concentration in solution related to As(III) oxidation of the three samples was observed after 30 min. This is due to formation of Mn(III) and re-adsorption of dissolved Mn^{2+} onto manganese oxides (Lafferty et al., 2011; Manning et al., 2002). We also compared Mn^{2+} formation rate (r_{Mn2+}) (Table 1). K-OMS-2-C revealed the highest r_{Mn2+} (7.76 μmol g^{-1} min^{-1}), followed by K-OMS-2-B (4.04 μmol g^{-1} min^{-1}) and then K-OMS-2-A (2.44 μmol g^{-1} min^{-1}). By increasing the K^+ concentration in OMS-2 tunnels, enhanced electron transfer from As to Mn stimulated As(III) oxidation as discussed above.

3.3.4 DFT calculation

To reveal K^+ effects on As(III) oxidation, As adsorption energy (E_{ads}) in the presence of varying K^+ concentrations (2 atom % and 4 atom % K^+) was calculated using density functional theory (DFT) calculations. Since H_2O molecules can rapidly adsorb on OMS-2 surfaces, this may affect As adsorption on OMS-2, so an OMS-2 model (~ 96 atoms) containing a H_2O molecule to simulate the solution system was created (Fig. 6). The As(V) species, $HAsO_4^{2-}$, were chosen to perform the calculations for this work. The formula for calculating adsorption energy (E_{ads}) of $HAsO_4^{2-}$ on K^+ doped OMS-2 was as follows.

$$E_{ads} = E_{total} - E_{bulk} - E_{HAsO42-}$$

Where E_{total} is the total energy of the K^+ doped OMS-2 supercell with a $HAsO_4^{2-}$ ion adsorbed, E_{bulk} is the bulk energy of the K^+ doped OMS-2 supercell, and $E_{HAsO42-}$ is the energy of a $HAsO_4^{2-}$ ion.

For OMS-2 supercells in the presence of low K^+ at 2 atom %, the obtained E_{ads} of $HAsO_4^{2-}$ was 5.94 eV. Increasing the K^+ concentration from 2 atom % to 4 atom %, the obtained E_{ads} of $HAsO_4^{2-}$ decreased from 5.94 eV to 4.69 eV. This indicated that high K^+ concentrations in the OMS-2 tunnel facilitates adsorption of $HAsO_4^{2-}$ ions on the OMS-2 supercell, which is in agreement with previous experimental work for As(V) adsorption.

The E_{ads} of As(III) species $HAsO_3^{2-}$ on the OMS-2 supercell with different K^+ concentrations in the tunnel was also calculated. The model for $HAsO_3^{2-}$ adsorption on OMS-2 surfaces was the same as that of $HAsO_4^{2-}$ adsorption (Fig. S7). The calculated E_{ads} of $HAsO_3^{2-}$ on the OMS-2 supercell in the presence of low K^+ concentration at 2 atom % was 7.21 eV,

which was greater than that in the presence of 4 atom % K^+ (6.27 eV), indicating that the presence of high K^+ concentrations makes adsorption of As(III) species on OMS-2 more favorable. The greater adsorption of As(III) on OMS-2 with high K^+ concentrations (e. g., 4 atom%), means that there is efficient contact between K-OMS-2 and As(III) species, which is a vital step before As(III) species are rapidly oxidized to As(V) by OMS-2.

To date, several strategies have been reported for improving As(III) oxidation on OMS-2. The first strategy involves decreasing particle size and increasing specific surface area (SSA) by synthesizing nano/micro-structured OMS-2 with tunable morphologies (Wang et al., 2012; Zhang and Sun, 2013). However, an increase in its specific As(III) oxidation rate was very low. The second strategy involved controlling reaction conditions by changing the system pH, temperature, initial As(III) concentration, and manganese oxide dosage (Fischel et al., 2015; Li et al., 2010). Nevertheless, manipulating pH, temperature, and As(III) concentration is very difficult to control in actual arsenic polluted groundwater, and the effect of reducing coexisting ions still remains unclear. A third strategy involves tuning the oxygen vacancy defect concentration in OMS-2 as reported in our previous work (Hou et al., 2016). The strategy described here, K^+ doping of OMS-2, is one of the most efficient methods to enhance arsenite oxidation, as evidenced by a considerable increase in As(III) oxidation rate and 3.8 times improvement in As(III) oxidation kinetic rate constants.

3.4 Environmental applications

Manganese oxide containing composites such as Fe and Mn enriched ore have been reportedly used as practicable adsorbent materials for treating actual arsenic contaminated groundwater in India and Brazil (Chakravarty et al., 2002; Deschamps et al., 2005). Batch and column experiments demonstrated the highly efficient adsorption capability of Fe and Mn enriched ore for As(III), mainly attributed to manganese oxides oxidation ability. Nevertheless, As(III) oxidation on Fe and Mn enriched ore is very slow due to the coating of manganese oxide surfaces by iron oxides, thus leading to the passivation of its active sites. Therefore, it is still necessary to utilize additional manganese oxides as low-cost and environmentally friendly oxidants for pre-oxidation of As(III) to As(V). However, it should not be ignored that the competitive adsorption effect can be passivated once it comes in to contact with abundant competitive ions and bacteria in aqueous environments. Therefore, rapid oxidation of arsenite to arsenate by K-OMS-2, and subsequent adsorption of produced arsenate by low cost natural Fe and Mn ore, is an available strategy for passivating

and decreasing toxicity of As species in arsenic contaminated groundwater, which will be further investigated in future work.

4 Conclusion

Cryptomelane-type manganese oxides with tunable K^+ concentrations were employed to remove arsenite from As-polluted water. Batch investigations revealed that the presence of high K^+ concentrations in OMS-2 greatly promoted As(III) oxidation activity and kinetic rates, thus reducing the unfavorable effects of coexisting ions such as As(V), phosphate, and Mn^{2+}. Experimental and theoretical evidence also revealed that increasing K^+ concentrations in OMS-2 led to highly efficient contact between manganese oxide and As species as well as fast charge transfer from As to Mn, thus considerably improving As(III) oxidation activity. The present work emphasizes the importance of rapid oxidation of highly toxic As(III) to less toxic As(V), when using manganese oxide containing composites as absorbent materials, especially in aqueous environments with abundant competitive ions. It is significant that all results presented here are from laboratory-based studies, and not from actual contaminated groundwater. Further studies are now required in order to assess the strategy described here using real arsenic contaminated wastewater.

Acknowledgment

This work was supported by the National Natural Science Foundation of China (41425006, 21707168), Natural Science Foundation of Hubei Province (2018CFB674). the Fundamental Research Funds for the Central Universities (No. 2662017QD013), China Postdoctoral Science Foundation (2015M580674), and Opening Foundation of the Chinese National Engineering Research Center for Control and Treatment of Heavy Metal Pollution, Changsha, 410083, China (No. 2015CNERC-CTHMP-03).

Appendix A. Supplementary data Supplementary

Appendix A. Supplementary data Supplementary data associated with this article can be found in the online version.

References

Chakravarty, S., Dureja, V., Bhattacharyya, G., Maity, S., Bhattacharjee, S., 2002. Removal of arsenic from groundwater using low cost ferruginous manganese ore. Water Res. 36, 625–632.

Chen, J., Wang, J., Zhang, G., Wu, Q., Wang, D., 2018. Facile fabrication of nanostructured cerium-manganese binary oxide

for enhanced arsenite removal from water. Chem. Eng. J. 334, 1518–1526.

Chiu, V.Q., Hering, J.G., 2000. Arsenic adsorption and oxidation at manganite surfaces. 1. Method for simultaneous of determination of adsorbed and dissolved arsenic species. Environ. Sci. Technol. 34, 2029–2034.

Deschamps, E., Ciminelli, V.S.T., Höll, W.H., 2005. Removal of As(III) and As(V) from water using a natural Fe and Mn enriched sample. Water Res. 39, 5212–5220.

Fischel, M.H.H., Fischel, J.S., Lafferty, B.J., Sparks, D.L., 2015. The influence of environmental conditions on kinetics of arsenite oxidation by manganese-oxides. Geochem. Trans. 16, 1–10.

Gorny, J., Billon, G., Lesven, L., Dumoulin, D., Madé, B., Noiriel, C., 2015. Arsenic behavior in river sediments under redox gradient: A review. Sci. Total Environ. 505, 423–434.

Gutiérrez-Ruíz, M., Villalobos, M., Romero, F., Fernández-Lomelín, P., 2005. Natural Attenuation of Arsenic in Semiarid Soils Contaminated by Oxidized Arsenic Wastes. Adv. Arsen. Res. ACS Symp. Ser.

Hou, J., Liu, L., Li, Y., Mao, M., Lv, H., Zhao, X., 2013. Tuning the K^+ concentration in the tunnel of OMS-2 nanorods leads to a significant enhancement of the catalytic activity for benzene oxidation. Environ. Sci. Technol. 47, 13730–13736.

Hou, J., Luo, J., Hu, Z., Li, Y., Mao, M., Song, S., Liao, Q., Li, Q., 2016. Tremendous effect of oxygen vacancy defects on the oxidation of arsenite to arsenate on cryptomelane-type manganese oxide. Chem. Eng. J. 306, 506–606.

Hou, J., Luo, J., Song, S., Li, Y., Li, Q., 2017a. The remarkable effect of the coexisting arsenite and arsenate species ratios on arsenic removal by manganese oxide. Chem. Eng. J. 315, 159–166.

Hou, J., Xiang, Y., Zheng, D., Li, Y., Xue, S., Wu, C., Hartley, W., Tan, W., 2017b. Morphology-dependent enhancement of arsenite oxidation to arsenate on birnessite-type manganese oxide. Chem. Eng. J. 327, 235–243.

Lafferty, B.J., Ginder-Vogel, M., Sparks, D.L., 2011. Arsenite oxidation by a poorly-crystalline manganese oxide. 3. Arsenic and manganese desorption. Environ. Sci. Technol. 45, 9218–9223.

Lafferty, B.J., Meade, T.G., Sparks, D.L., 2010. Evaluating Environmental Influences on As III Oxidation Kinetics by a Poorly Crystalline Mn-Oxide. Environ. Sci. Technol. 44, 3772–3778.

Lan, S., Ying, H., Wang, X., Liu, F., Tan, W., Huang, Q., Zhang, J., Feng, X., 2018. Efficient catalytic As(III) oxidation on the surface of ferrihydrite in the presence of aqueous Mn(II). Water Res. 128, 92–101.

Li, X. juan, Liu, C. shuai, Li, F. bai, Li, Y. tao, Zhang, L. jia, Liu, C. ping, Zhou, Y. zhang, 2010. The oxidative transformation of sodium arsenite at the interface of α-MnO2 and water. J. Hazard. Mater. 173, 675–681.

Liu, J., Makwana, V., Cai, J., Suib, S.L., Aindow, M., 2003. Effects of Alkali Metal and Ammonium Cation Templates on Nanofibrous Cryptomelane-type Manganese Oxide Octahedral Molecular Sieves (OMS-2). J. Phys. Chem. B 107, 9185–9194.

Luo, J., Zhu, H.T., Liang, J.K., Rao, G.H., Li, J.B., Du, Z.M., 2010. Tuning Magnetic Properties of α-MnO_2 Nanotubes by K^+ Doping 8782–8786.

Maliyekkal, S.M., Philip, L., Pradeep, T., 2009. As(III) removal from drinking water using manganese oxide-coated-alumina: Performance evaluation and mechanistic details of surface binding. Chem. Eng. J. 153, 101–107.

Manning, B.A., Fendorf, S.E., Bostick, B., Suarez, D.L., 2002. Arsenic(III) oxidation and arsenic(V) adsorption reactions on synthetic birnessite. Environ. Sci. Technol. 36, 976–981.

Mondal, P., Bhowmick, S., Chatterjee, D., Figoli, A., Van der Bruggen, B., 2013. Remediation of inorganic arsenic in groundwater for safe water supply: A critical assessment of technological solutions. Chemosphere 92, 157–170.

Moore, J.N., Walker, J.R., Hayes, T.H., 1990. As (III) TO As (V) BY BIRNESSITE. Clays Clay Miner. 38, 549–555.

Nesbitt, H.W., Canning, G.W., Bancroft, G.M., 1998. XPS study of reductive dissolution of 7Å-birnessite by H3AsO3, with constraints on reaction mechanism. Geochim. Cosmochim. Acta.

Neumann, A., Kaegi, R., Voegelin, A., Hussam, A., Munir, A.K.M., Hug, S.J., 2013. Arsenic removal with composite iron matrix filters in Bangladesh: A field and laboratory study. Environ. Sci. Technol. 47, 4544–4554.

Smedley, P.L., Kinniburgh, D.G., 2002. A review of the source, behaviour and distribution of arsenic in natural waters. Appl. Geochemistry 17, 517–568.

Ventura-Lima, J., Bogo, M.R., Monserrat, J.M., 2011. Arsenic toxicity in mammals and aquatic animals: A comparative biochemical approach. Ecotoxicol. Environ. Saf. 74, 211–218.

Villalobos, M., Escobar-Quiroz, I.N., Salazar-Camacho, C., 2014. The influence of particle size and structure on the sorption and oxidation behavior of birnessite: I. Adsorption of As(V) and oxidation of As(III). Geochim. Cosmochim. Acta 125, 564–581.

Wan, B., Yan, Y., Liu, F., Tan, W., He, J., Feng, X., 2016. Surface speciation of myo-inositol hexakisphosphate adsorbed on TiO2 nanoparticles and its impact on their colloidal stability in aqueous suspension: A comparative study with orthophosphate. Sci. Total Environ. 544, 134–142.

Wang, M., Tan, W., Feng, X., Koopal, L.K., Liu, M., Liu, F., 2012. One-step synthesis of sea urchin-like α-MnO 2 using KIO 4 as the oxidant and its oxidation of arsenite. Mater. Lett. 77, 60–62.

Yan, Y., Li, W., Yang, J., Zheng, A., Liu, F., Feng, X., Sparks, D.L., 2014. Mechanism of myo-inositol hexakisphosphate sorption on amorphous aluminum hydroxide: Spectroscopic evidence for rapid surface precipitation. Environ. Sci. Technol. 48, 6735–6742.

Zhang, G., Khorshed, A., Paul Chen, J., 2013. Simultaneous removal of arsenate and arsenite by a nanostructured zirconium-manganese binary hydrous oxide: Behavior and mechanism. J. Colloid Interface Sci. 397, 137–143.

Zhang, G., Liu, F., Liu, H., Qu, J., Liu, R., 2014. Respective role of Fe and Mn oxide contents for arsenic sorption in iron and manganese binary oxide: An X-ray absorption spectroscopy investigation. Environ. Sci. Technol. 48, 10316–10322.

Zhang, G., Qu, J., Liu, H., Liu, R., Wu, R., 2007. Preparation and evaluation of a novel Fe-Mn binary oxide adsorbent for effective arsenite removal. Water Res. 41, 1921–1928.

Zhang, T., Sun, D.D., 2013. Removal of arsenic from water using multifunctional micro-/nano-structured MnO2 spheres and microfiltration. Chem. Eng. J. 225, 271–279.

Zhu, M., Paul, K.W., Kubicki, J.D., Sparks, D.L., 2009. Quantum chemical study of arsenic (III, V) adsorption on Mn-oxides: Implications for arsenic(III) oxidation. Environ. Sci. Technol. 43, 6655–6661.

List of Table and Figure captions

Table 1 Specific surface area, specific As(III) oxidation rate within 5min, and initial Mn^{2+} release rate of the samples.

Fig. 1. The evolution of As(III) concentration with reaction time in solution duing reaction between 1.2 g L^{-1} OMS-2 sample and 100 μM As(III) solution at pH 6.0 (A) and the fitting result of As(III) oxidation kinetics on different samples using a first-order kinetics equation (B).

Fig. 2. A(III) removal before and after addition of 100 μM As(V) (A) and As (V) adsorption on K^+ doped OMS-2 at pH 6.0 (B): OMS-2 dosage was 1.2 g L^{-1}, As(V) concentraiton was 100 μM.

Fig. 3. As(III) removal with and without addition of 100 μM phosphate (green column) and Mn^{2+} (blue column) during reaction between 100 μM As(III) and 1.2 g L^{-1} sample at pH 6.0 (A) and fitting curves for phosphate adsorption kinetics on three samples at 100 μM phosphate concentration and 1.2 g L^{-1} dosage.

Fig. 4. Zeta potentials of the samples as a function of pH value of suspensions.

Fig. 5. Change of dissolved Mn^{2+} concentration with reaction time during recation between 100 μM As(III) solution and 1.2 g L^{-1} OMS-2 at pH 6.0.

Fig. 6. Calculated supercell of K^+ doped OMS-2 with 2 atom % K^+ ($K_2Mn_{32}O_{64}$) (a) and 4 atom % K^+ ($K_4Mn_{32}O_{64}$) (b): $HAsO_4^{2-}$ ion and H_2O molecule adsorbed at the surface of the supercell.

Table 1 Specific surface area, specific As(III) oxidation rate within 5min, and initial Mn^{2+} release rate of the samples.

Samples	Surface area (m^2 g^{-1})	K/Mn atomic ratio		As(III) reaction rate (μmol g^{-1} min^{-1})	Specific As(III) reaction rate (μmol m^{-2} min^{-1})	r_{Mn2+} (μmol g^{-1} min^{-1})
		ICP-OES	XPS			
K-OMS-2-A	65.1	0	0	2.90	0.045	7.76
K-OMS-2-B	89.2	0.03	0.04	4.29	0.048	4.04
K-OMS-2-C	109.7	0.07	0.08	7.78	0.071	2.44

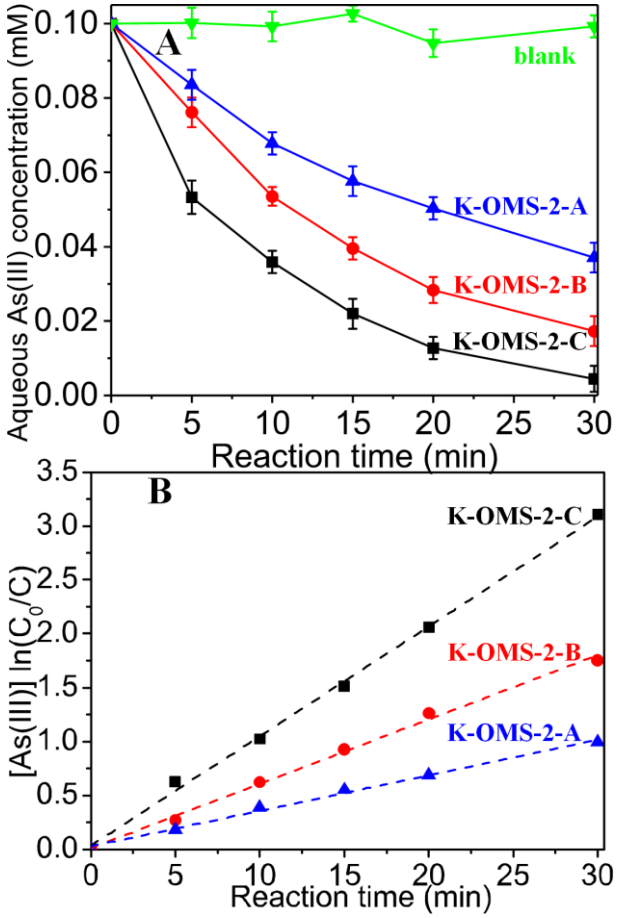

452

453 **Fig. 1**. Evolution of As(III) concentration with reaction time in solution duing reaction between 1.2 g L^{-1} OMS-2 and 100

454 μM As(III) at pH 6.0 (A) (green line represents blank test of As(III) oxidation in the absence of OMS-2), and the fitting

455 result of As(III) oxidation kinetics on different samples using a first-order kinetics equation (B).

456

457

458 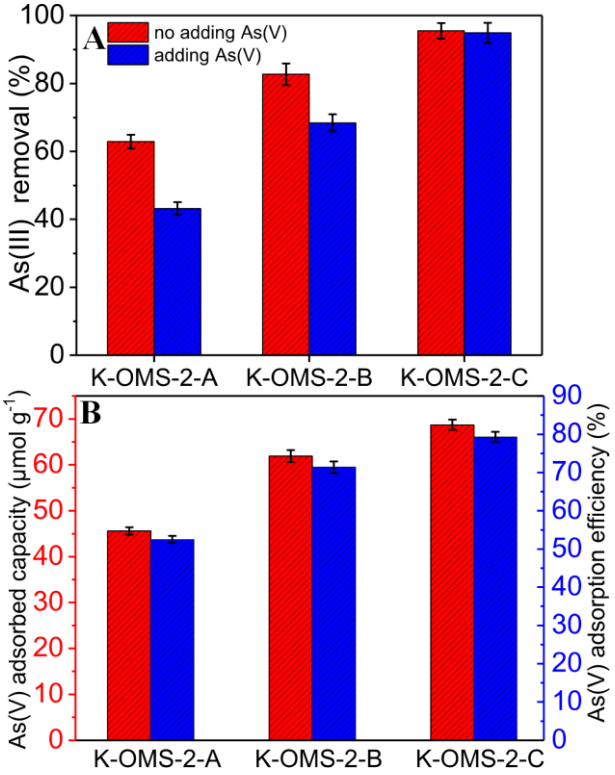

459 **Fig. 2.** As(III) removal before and after addition of 100 μM As(V) (A) and As (V) adsorption on K^+ doped OMS-2 at pH

460 6.0 (B): OMS-2 dosage was 1.2 g L^{-1}, As(V) concentraiton was 100 μM.

461

462

463

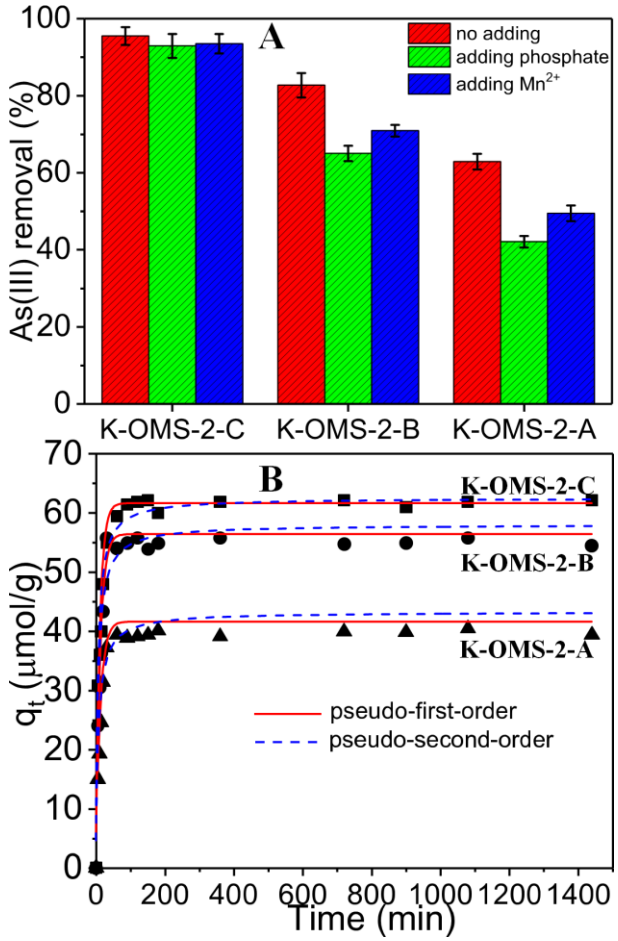

Fig. 3. As(III) removal with and without addition of 100 μM phosphate (green column) and Mn^{2+} (blue column) during reaction between 100 μM As(III) and 1.2 g L^{-1} sample at pH 6.0 (A) and fitting curves for phosphate adsorption kinetics on three samples at 100 μM phosphate concentration and 1.2 g L^{-1} dosage.

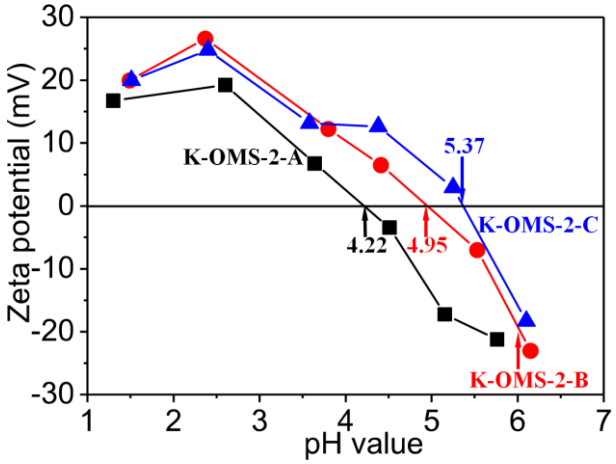

Fig. 4. Zeta potentials of the samples as a function of suspension pH.

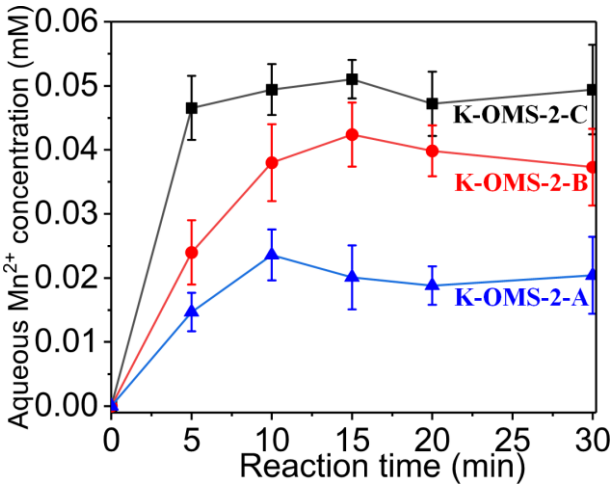

475

476 **Fig. 5.** Change of dissolved Mn^{2+} concentration with reaction time during recation between 100 μM As(III) solution

477 and 1.2 g L^{-1} OMS-2 at pH 6.0.

478

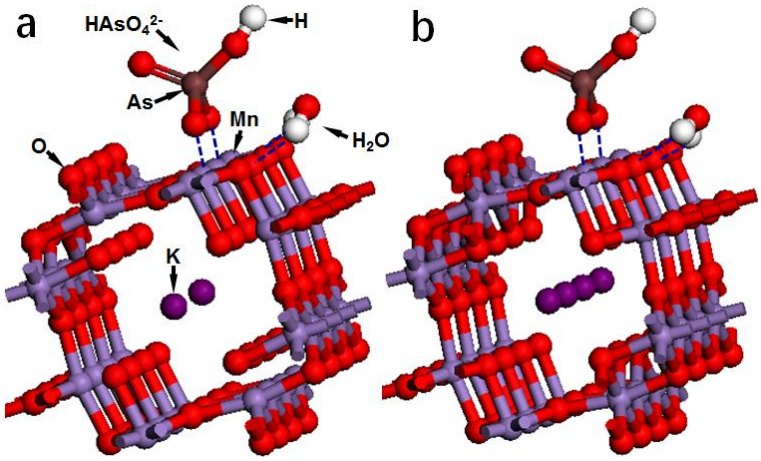

479

480 **Fig. 6.** Calculated supercell of K^+ doped OMS-2 with 2 atom % K^+ ($K_2Mn_{32}O_{64}$) (a) and 4 atom % K^+ ($K_4Mn_{32}O_{64}$) (b):

481 $HAsO_4^{2-}$ ion and H_2O molecule adsorbed at the surface of the supercell.

482